Systematic study of FIB-induced damage for the high-quality TEM sample preparation

Jun Uzuhashi* and Tadakatsu Ohkubo

National Institute for Materials Science, Tsukuba, 305-0047, Japan

**Corresponding author. E-mail: UZUHASHI.Jun@nims.go.jp*

Keywords: FIB; focused ion beam, (S)TEM; (scanning) transmission electron microscopy

Abstract

Nowadays, a focused Ga ion beam (FIB) with a scanning electron microscopy (SEM) system has been widely used to prepare the thin-foil sample for transmission electron microscopy (TEM) or scanning TEM (STEM) observation. An establishment of a solid strategy for a reproducible high-quality sample preparation process is essential to carry out high-quality (S)TEM analysis. In this work, the FIB damages introduced by Ga^+ beam were investigated both experimentally and stopping and range of ions in matter (SRIM) simulation for silicon (Si), gallium nitride (GaN), indium phosphide (InP), and gallium arsenide (GaAs) semiconductors. It has been revealed that experimental investigations of the FIB-induced damage are in good agreement with SRIM simulation by defining the damage as not only "amorphization" but also "crystal distortion". The systematic evaluation of FIB damages shown in this paper should be indispensable guidance for reliable (S)TEM sample preparation.

Introduction

Transmission electron microscopy (TEM) or scanning TEM (STEM) is the major technique to investigate materials and devices on the atomic scale [1, 2]. The invention of spherical aberration (C_s) corrected (S)TEM in the late 1990s to 2000s contributed to the technique becoming a much more powerful tool for microstructural analyses [3-7]. An introduction and establishment of the TEM sample preparation method using a focused Ga ion beam (FIB) with a scanning electron microscopy (SEM) system have made a great impact on site-specific cross-sectional and plan-view TEM sample preparation [8-14]. In recent years, several automated FIB fabrications have been also demonstrated and are under development for reproducible, high throughput, and statistical research work [15-21]. The "*AutoTEM5*" program developed by *Thermo Fisher Scientific* enables fully automated lift-out and thinning processes by pre-defined FIB fabrication parameters [18, 19]. *CarlZeiss* has also developed "*SmartEPD* (end-point-detection)" program on CrossBeam FIB-SEM systems to judge the end point of FIB fabrication [16]. On the other hand, C_s-corrected (S)TEM instrument seriously requires a uniform thin-foil (S)TEM sample (hereafter, we will refer to just "TEM sample") with minimized FIB-induced damage. However, it is well known that the FIB, Ga^+ beam, induces damage into the materials, destroying the crystal structures and making them amorphous [10, 11]. A low keV FIB milling is known to be effective in reducing FIB damage [11, 22-28]. Thus, a higher keV FIB milling is generally selected in the beginning, and then low keV beams are used for the final thinning process. In the several steps of the FIB thinning process, it is key to understand how much damage is introduced by the chosen FIB beam condition at each step regardless of cross-sectional or plan-view samples. Also in automated sample preparation, the selection of pre-defined FIB milling conditions determines the quality of the sample. Thus, it should be time to evaluate the FIB damage systematically to improve

the reproducibility and reliability of TEM sample preparation. This work focuses on the experimental investigation of the FIB-induced damage with a comparison of previous reports, and the discussion between experimental results and the simulation. The systematic evaluation of FIB damage leads to the development of a solid strategy for a reproducible high-quality TEM sample preparation process.

Methods and Materials

A FIB-SEM dual beam system, Helios 5UX (*Thermo Fisher Scientific*), was used in the experiment. The evaluation of FIB damage, in other words, the FIB-damaged layer formed on the sample's side surface was investigated by Titan G2 80-200 (*Thermo Fisher Scientific*) at 200 keV. The scheme of how to evaluate the thickness of FIB damage is the same or similar method used in previous studies [11, 22, 24-29]. The side wall surface of the target material was milled by FIB first, then the damaged surface was capped with Pt electron beam deposition, followed by a thinning process to the TEM sample. The FIB beams of 30 keV: 90 pA, 8 keV: 61 pA, 5 keV: 63 pA, and 2 keV: 66 pA were used to fabricate the side walls. By the cross-sectional (S)TEM observation, the FIB-damaged layer is investigated experimentally. In addition to the experimental evaluation, the Ga ion implantation (I/I) depth can be simulated by stopping and range of ions in matter (SRIM) programs developed by Ziegler [30, 31]. The SRIM can calculate the interaction between the implanted ion and the target material [31]. In this study, the simulation results at Ga^+ ion accelerating voltages of 30 keV, 8 keV, 5 keV, and 2 keV were calculated. The incident angle of Ga ions was set as 89.5 degrees, close to the actual FIB thinning process. In this way, the dependence between Ga I/I and its accelerating voltage can be simulated by the SRIM program [31]. As target materials, Si (a widely used semiconductor), indium phosphide (InP; commonly used semiconductor as

a substrate for laser applications), gallium nitride (GaN; a promising candidate for the next-generation power devices), and gallium arsenide (GaAs; a semiconductor used in the integrated circuits) were selected and evaluated in this study.

Experimental Results

Figure 1(a) shows a schematic workflow of how to evaluate FIB-induced damage, a detailed method can be found in previous reports [11, 22, 24-29]. The cross-sectional low-angle annular dark-field (LAADF-) STEM image of the 30 keV FIB damage on the Si is shown in **Fig. 1(b)**. As confirmed by nano-beam electron diffraction (NBD) analysis as shown in **Fig. 1(c)**, the amorphous layer of ~22 nm was formed on the surface by FIB. **Fig. 1(d)** shows the Ga compositional profile obtained by STEM-EDS (red-colored dotted line) and the intensity profile of the LAADF-STEM image (black-colored line, obtained from integrating multiple lines with approximately 200 pm width, see **Suppl Fig. 1**) as a function of the depth. Note that the EDS line profile was calculated by 50-nm-width integration. The Ga composition is 0.5 ~ 2.0 at% up to ~12 nm and then gradually decreases in the depth direction. When the Ga concentration increases above a certain value, it seems that amorphization occurs. As seen in the intensity profile of the STEM image, a periodicity started to be recognized from ~22 nm depth, indicating Si remained as a crystal structure. It should be noted that a brighter contrast appeared from ~22 to ~29 nm depth in the crystal region as indicated by blue-colored arrows in **Fig. 1(b) and (d)**. There is no compositional change, *i.e.,* Ga increase, at the region with the brighter contrast. This brighter contrast in the crystal region will be discussed later.

Figure 2(a) shows the LAADF-STEM images with different accelerating FIB voltages, and **Fig. 2(b)** shows the intensity profiles of the STEM image as a function of the depth. The amorphized layer thicknesses are ~22 nm (30 keV), ~7 nm (8 keV), ~4 nm (5 keV), and ~1 nm

(2 keV), respectively. These values are plotted in **Fig. 2(b)** as red-colored circles, also showing values reported in previous studies [10, 22, 24, 26, 28]. The thicknesses of the amorphous layer are slightly region-dependent; therefore, the error bars are drawn by the maximum and minimum depths. Figures shown later also contain error bars in the same way. Although FIB systems are different from each other, all the results are consistent. This means that our experimental method can well reproduce previous studies. This fact confirms the report by Kato *et al.* [26], that is, the FIB-damaged amorphous thickness is changed by accelerating voltage irrespective of the beam current.

There are several reports on FIB damage on Si, however, few studies can be found for other materials to the best of our knowledge. Thus, some other materials were investigated by using the same method. **Figure 3** shows LAADF-STEM images of GaN, InP, and GaAs and the amorphization depths. Note that the left side in all the images is the side surface milled by FIB. As the same as the Si case, amorphous layers were recognized in STEM images for all the materials and voltages. In addition to amorphization, brighter contrasts in the crystal region were also observed as the same as Si. Thicknesses of amorphous are summarized in **Fig. 3(d)-(f)** with previous reports [25, 29]. The GaN results are much smaller than the previous report by Sato *et al.* [29] because they defined the FIB damage based on the diffraction contrast in the bright-field TEM images not from amorphous thickness.

The simulated depth of Ga I/I for Si, GaN, InP, and GaAs with different accelerating FIB voltages are plotted in **Figure 4** [31]. **Fig. 4(a)** shows a schematic in the case of the Ga^+ of 8 keV being implanted into Si. The black dot lines indicate Ga I/I trajectories in the Si bulk. From the simulated stopping position of implanted Ga^+, Ga^+ distribution as a function of the depth direction can be plotted as indicated by the red-colored histogram in **Fig. 4(b)**. Although only 300 ions are shown in **Fig. 4(a) and (b)** for better visualization, 10,000 ions were simulated

in the calculation for **Fig. 4(c)-(f)**. The values in the parentheses written at each voltage indicate the depth of Ga I/I. The Ga I/I depth is defined as the depth of 99% of ions implanted into the material here.

Discussions

Comparing **Fig. 2, 3, and 4**, the amorphous thicknesses caused by FIB are in good agreement in the Si case; however, these values for GaN, InP, and GaAs always show much lower values than the Ga I/I depth. The FIB damage has been mainly defined and investigated as amorphization conventionally; however, we should not treat the FIB damage only as "amorphization". As mentioned earlier, Sato *et al.* reported the FIB damage as the diffraction contrast in the TEM image, indicating the crystal distortion [29]. Whereas high-angle ADF (HAADF)-STEM images are sensitive to atomic number Z, the contrast of LAADF-STEM images used in this work is also affected by crystal distortions [32]. By using the contrast of the LAADF-STEM imaging technique, the visualization of GaN crystal distortion has been reported [33]. Thus, the brighter contrasts in the LAADF-STEM images near the amorphous/crystal interfaces as indicated by blue-colored arrows in **Fig. 1(b) and (d)** should be considered as a part of FIB damage. As seen in **Fig. 2 and Fig. 3**, brighter contrasts are always observed for all the materials even at the lower keV FIB fabrications. The intensity profiles of LAADF-STEM images of GaN, InP, and GaAs were also plotted in the same way as the Si case (**Suppl Fig. 2**). If including the thickness of the bright contrast in addition to the amorphous layer, the results become as shown in **Figure 5** [10, 22, 24-26, 28, 29, 31]. These values (red-colored stars) are in good agreement with Ga I/I depth (black-colored squares) calculated by SRIM. Thus, it should be concluded that "FIB damage" consists of "amorphization" and "crystal distortion" layers. The crystal distortion can be caused by the

atom displacements or vacancy formations by Ga I/I. The ratios of (amorphous thickness)/(total FIB damage, that is, the total thickness of amorphous and crystal distortion regions) at 30 keV are ~75% (Si), ~13% (GaN), ~67% (InP), and ~68% (GaAs). The amount of Ga I/I would be varied by FIB milling yield, and the underlying amorphization mechanism should be related to the crystal stability against the Ga I/I and the temperature increase caused by FIB, and so on; thus, further consideration is required for understanding these differences. The cryo-stage FIB system may help in understanding whether the Ga I/I induced heating has an effect or not on the amorphization at least, but it's future work.

The FIB is a powerful technique for preparing TEM samples in a wide range of materials. To prepare a high-quality TEM sample, the FIB damage should be minimized. Without the knowledge of the FIB damage, the TEM sample preparation would be groping in the dark. The SRIM simulation would give operators a useful prediction for the damage thickness induced by the Ga^+ beam, leading to a solid strategy for high-quality TEM sample preparation. Also, for the development of automated sample preparation, the selection of pre-defined FIB beams will deeply determine the sample quality. If we add a few, the microfabrication by using an Xe plasma FIB system has been recently developed, and Xe-induced damage is smaller by experimental reports and SRIM simulation [28, 29]. The low keV Ar ion milling is also reported effective in removing the FIB-induced damages [25, 29, 34], for this purpose, the FIB-SEM-Ar triple beam system has been commercialized by *Hitachi High-Tech* [29]. We should carefully select suitable preparation techniques depending on the purpose of (S)TEM investigations.

Conclusion

In summary, we systematically evaluated the damages induced by FIB for Si, GaN,

InP, and GaAs. Conventionally, FIB-induced damage has been mainly evaluated from the viewpoint of amorphized thickness. In this work, cross-sectional LAADF-STEM observation on the FIB milled surfaces has revealed that "FIB damage" is not only "amorphization" but also "crystal distortion" caused by Ga I/I. The systematic study of the FIB damage is a great guide for the establishment of a solid strategy to prepare the high-quality TEM sample. Especially for the ultra-thin TEM samples, the FIB damage critically influences cutting-edge (S)TEM investigations. Furthermore, the optimized procedure to prepare TEM samples will strongly contribute to improving the reproducibility and reliability of (S)TEM analyses themselves.

Figure 1

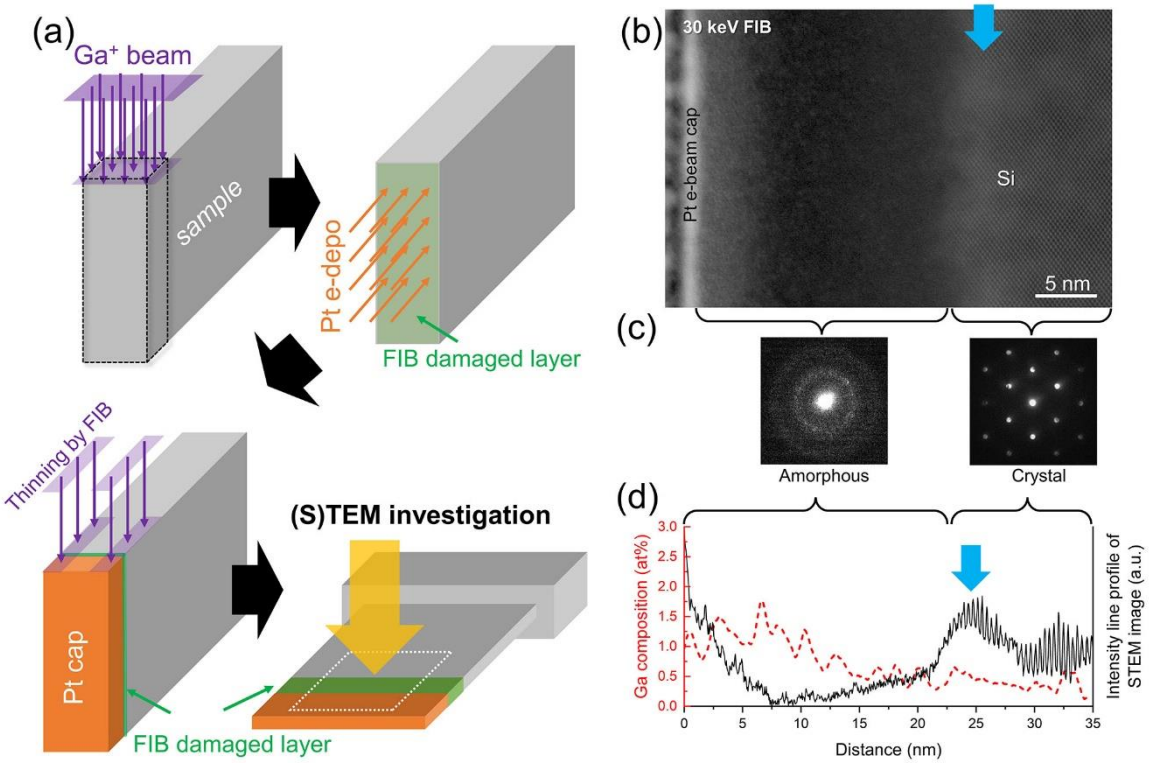

Figure 1. (a) Schematic workflow of how to evaluate FIB damage. Milling the material by Ga^+ beam, capping the FIB damaged surface (indicated by green color) with Pt electron beam deposition (indicated by orange color), and then thinning to TEM sample. Observing the damage by the TEM technique. (b) Cross-sectional LAADF-STEM image of 30 keV FIB milled surface of Si crystal. (c) NBD patterns of the amorphous layer and Si crystal. (d) The Ga compositional profile obtained by STEM-EDS (red-colored dotted line) and the intensity profile of the LAADF-STEM image (black-colored line) as a function of the depth.

Figure 2

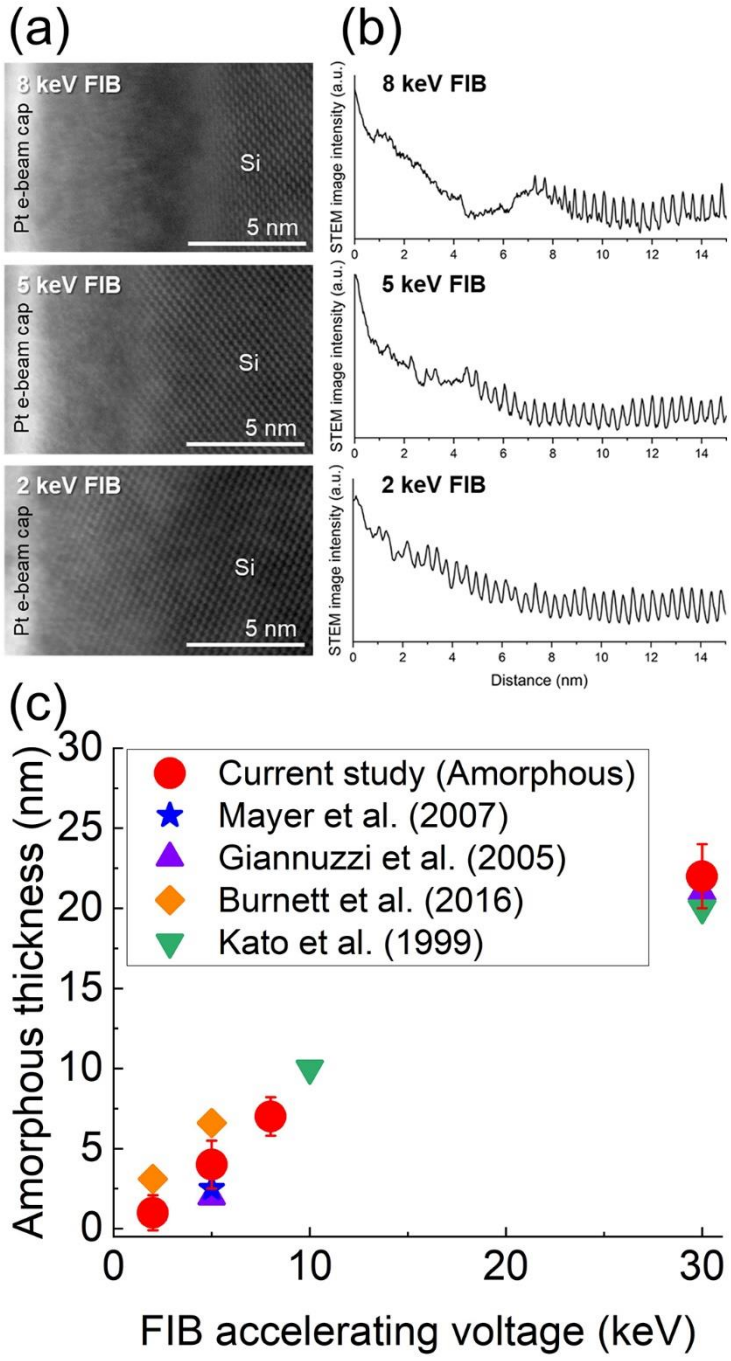

Figure 2. (a) Cross-sectional LAADF-STEM images of Si's side wall surface after FIB milling at 8, 5, and 2 keV. (b) The intensity profiles of the LAADF-STEM image as a function of the depth. (c) The amorphous layer thicknesses in Si with different accelerating FIB voltages. Previous studies are also plotted in the figure [10, 22, 24, 26, 28].

Figure 3

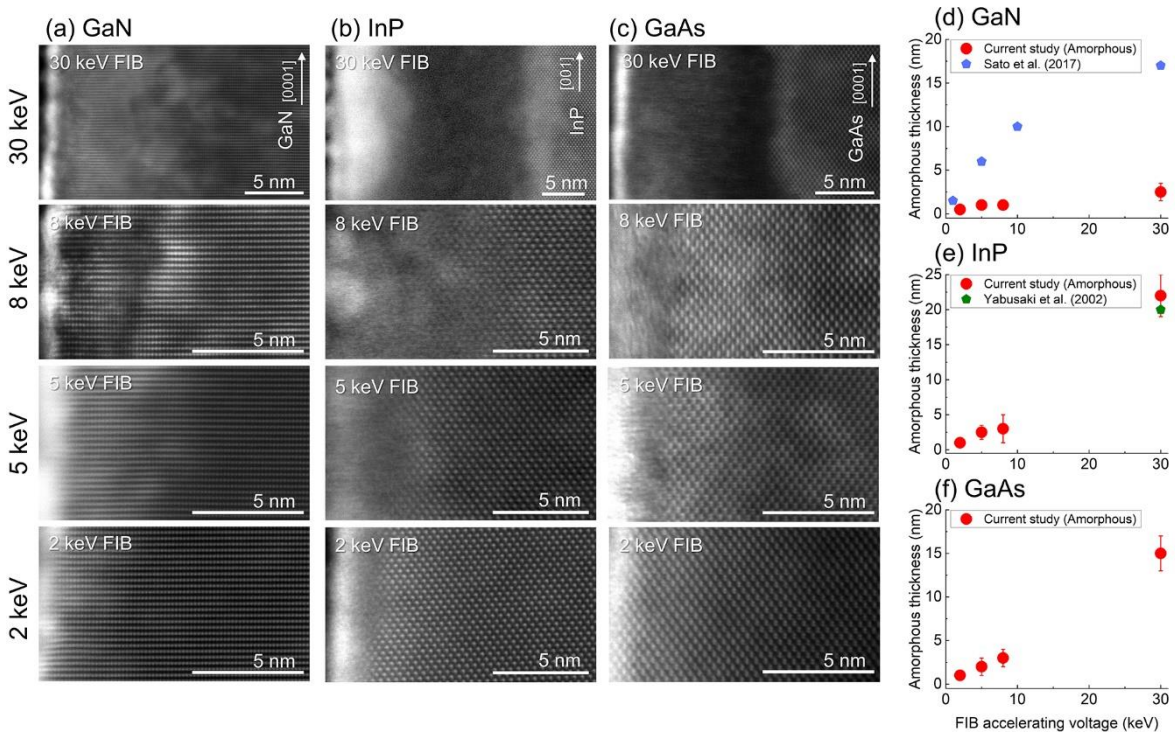

Figure 3. Cross-sectional LAADF-STEM images of the side wall surface milled by FIB with different accelerating voltages for (a) GaN, (b) InP, and (c) GaAs. Note that the side wall surface is the left side in all the images. The amorphized depths for (d) GaN, (e) InP, and (f) GaAs [25, 29]. Note that a previous study on GaN by Sato *et al.* reported the thicknesses of crystal distortion [29].

Figure 4

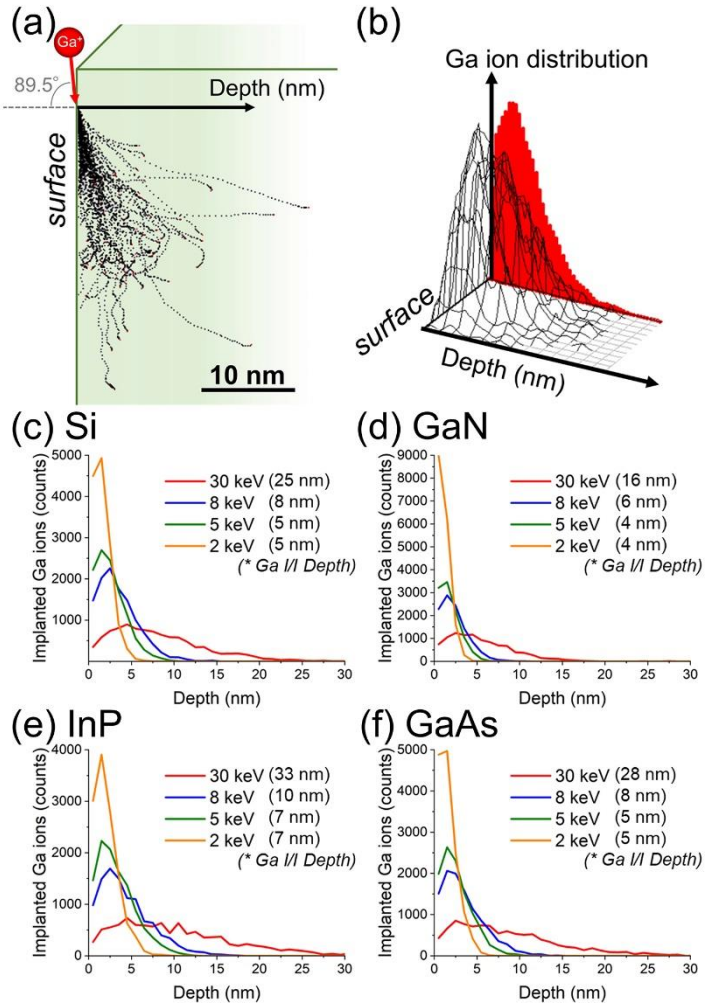

Figure 4. (a) Schematic of SRIM simulation in the case of the Ga^+ of 8 keV being implanted into silicon (Si). The black dot lines indicate trajectories of implanted Ga ions into the Si. (b) Ga ions count as a function of the implanted depth is plotted by a red-colored histogram. Both images of (a) and (b) were generated SRIM program [31], and arranged for better visualization by the authors. The calculated depth distribution of 10,000 implanted Ga^+ for (c) Si, (d) GaN, (e) InP, and (f) GaAs with different accelerating voltages. The depth of Ga I/I is defined as the depth that 99% of ions implanted into the material and the counts are calculated with 1 nm steps here.

Figure 5

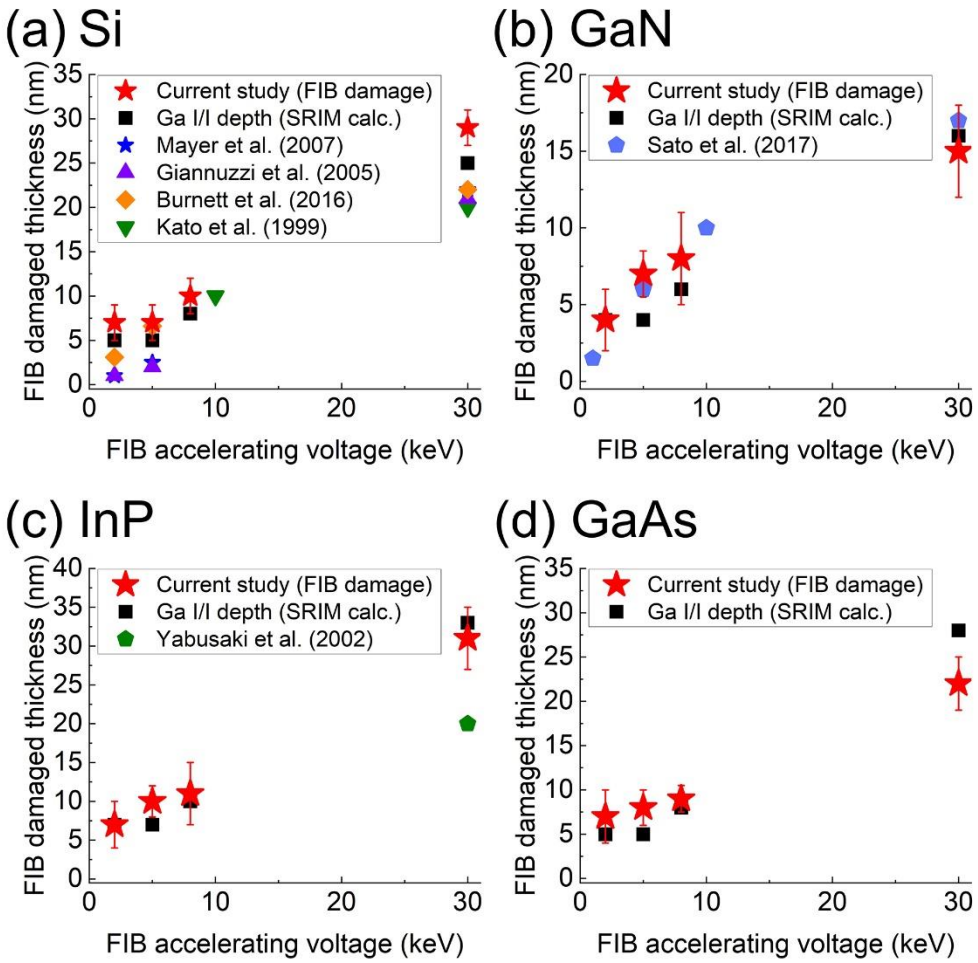

Figure 5. FIB damage thicknesses as defined as the total of amorphization and crystal-distortion, (red-colored stars), the Ga I/I depths by SRIM simulation (black-colored squares) for (a) Si, (b) GaN, (c) InP, and (d) GaAs [10, 22, 24-26, 28, 29, 31].

References

1. D.B. Williams and C.B. Carter, Transmission Electron Microscopy - A Textbook for Materials Science -, Springer New York, NY (1996). https://doi.org/10.1007/978-1-4757-2519-3
2. H. Kohl and L. Reimer, Transmission electron microscopy - physics of image formation and microanalysis -, Springer New York, NY (2008). https://doi.org/10.1007/978-0-387-40093-8
3. M. Haider, H. Rose, S. Uhlemann, E. Schwan, B. Kabius, K. Urban, A spherical-aberration-corrected 200 kV transmission electron microscope, Ultramicroscopy **75** (1998), 53-60. https://doi.org/10.1016/S0304-3991(98)00048-5
4. M Haider, S Uhlemann, E Schwan, H Rose, B Kabius, K Urban, Electron microscopy image enhanced, Nature **392** (1998), 768-769. https://doi.org/10.1038/33823
5. O.L. Krivanek, N. Dellby, A.R. Lupini, Towards sub-Å electron beams, Ultramicroscopy **78** (1999), 1-11. https://doi.org/10.1016/S0304-3991(99)00013-3
6. OL Krivanek, PD Nellist, N Dellby, MF Murfitt, Z Szilagyi, Towards sub-0.5 Å electron beams, Ultramicroscopy **96** (2003), 229-237. https://doi.org/10.1016/S0304-3991(03)00090-1
7. K.W. Urban, Studying atomic structures by aberration-corrected transmission electron microscopy, Science **321** (2008), 506-510. https://doi.org/10.1126/science.1152800
8. L.A. Giannuzzi, F.A. Stevie, A review of focused ion beam milling techniques for TEM specimen preparation, Micron **30** (1999), 197-204. https://doi.org/10.1016/S0968-4328(99)00005-0
9. C. A. Volkert and A. M. Minor, Focused Ion Beam Microscopy and Micromachining, MRS Bulletin **32** (2007), 389-399. https://doi.org/10.1557/mrs2007.62

10. J. Mayer, L.A. Giannuzzi, T. Kamino, J. Michael, TEM sample preparation and FIB-induced damage, MRS Bulletin **32** (2007), 400-407. https://doi.org/10.1557/mrs2007.63
11. M. Schaffer, B. Schaffer, Q. Ramasse, Sample preparation for atomic-resolution STEM at low voltages by FIB, Ultramicroscopy **114** (2012), 62-71. https://doi.org/10.1016/j.ultramic.2012.01.005
12. F. Lenrick, M. Ek, D. Jacobsson, M.T Borgström, L R. Wallenberg, FIB Plan and Side View Cross-Sectional TEM Sample Preparation of Nanostructures, Microscopy and Microanalysis **20**, 133-140 (2014). https://doi.org/10.1017/S1431927613013780
13. L-H. Le, C-H. Yu, C-Y. Wei, P-C. Lee, J-S. Huang, C-Y. Wen, Plan-view transmission electron microscopy specimen preparation for atomic layer materials using a focused ion beam approach, Ultramicroscopy **197**, 95-99 (2019). https://doi.org/10.1016/j.ultramic.2018.12.001
14. N.S Rajput, K. Sloyan, D.H. Anjum, M. Chiesa, A. Al Ghaferi, A user-friendly FIB lift-out technique to prepare plan-view TEM sample of 2D thin film materials, Ultramicroscopy **235**, 113496 (2022). https://doi.org/10.1016/j.ultramic.2022.113496
15. T. Volkenandt, A. Laquerre, M. Postolski, F. Pérez-Willard, Automatic FIB-SEM Preparation of Straight Pillars for In-Situ Nanoindentation, Microscopy and Microanalysis **22** (2016), 190-191. https://doi.org/10.1017/S143192761600180X
16. T. Volkenandt, F. Pérez-Willard, M. Rauscher, P.M. Anger, Towards Automatic Lamella Thinning Using Live Thickness Measurements and Smart End-Point Detection, Microscopy and Microanalysis **23** (2017), 304-305. https://doi.org/10.1017/S1431927617002203
17. B.V. Leer, R. Geurts, R. Scharfschwerdt, H. Cheng, L. Li, and R. Imlau, New Workflows Broaden Access to S/TEM Analysis and Increase Productivity, Microsc. Today **26** (2018),

18–25. https://doi.org/10.1017/S1551929517001195

18. M. Dutka1 and A. Prokhodtseva, AutoTEM 5 – Fully Automated TEM Sample Preparation for Materials Science, Microscopy and Microanalysis **25** (2019), 554-555. https://doi.org/10.1017/S1431927619003507
19. H. Tsurusawa, N. Nakanishi, K. Kawano, Y. Chen, M. Dutka, B.V. Leer and T. Mizoguchi, Robotic fabrication of high-quality lamellae for aberration-corrected transmission electron microscopy, Scientific Reports **11** (2021), 21599. https://doi.org/10.1038/s41598-021-00595-x
20. M. Dutka, B.V. Leer, H. Tsurusawa, N. Nakanishi, K. Kawano, Y. Cheng and T. Mizoguchi, Robotic Fabrication of High-quality Lamellae for Aberration-corrected Transmission Electron Microscopy, Microscopy and Microanalysis **28** (2022), 54. https://doi.org/10.1017/S1431927622001131
21. J. Uzuhashi, T. Ohkubo, and K. Hono, Development of automated tip preparation for atom probe tomography by using script-controlled FIB-SEM, Ultramicroscopy **247** (2023), 113704. https://doi.org/10.1016/j.ultramic.2023.113704
22. L.A. Giannuzzi, R. Geurts, and J. Ringnalda, 2 keV Ga+ FIB Milling for Reducing Amorphous Damage in Silicon, Microscopy and Microanalysis **11** (2005), 828-829. https://doi.org/10.1017/S1431927605507797
23. K. Thompson, B. Gorman, D. J. Larson, B. van Leer and L. Hong, Minimization of Ga Induced FIB Damage Using Low Energy Clean-up, Microscopy and Microanalysis **12** (2006), 1736-1737. https://doi.org/10.1017/S1431927606065457
24. L.A. Giannuzzi, Reducing FIB Damage Using Low Energy Ions, Microscopy and Microanalysis **12** (2006), 1260-1261. https://doi.org/10.1017/S1431927606065469
25. K. Yabusaki and H. Sasaki, Specimen Preparation Technique for a Microstructure Analysis

Using the Focused Ion Beam Process, Furukawa Review **22** (2002). https://www.furukawa.co.jp/review/fr022/fr22_13.htm

26. N.I. Kato, Y. Kohno, H. Saka, Side-wall damage in a transmission electron microscopy specimen of crystalline Si prepared by focused ion beam etching, Journal of Vacuum Science & Technology A **17** (1999), 1201. https://doi.org/10.1116/1.581795
27. N.I. Kato, Reducing focused ion beam damage to transmission electron microscopy samples, Journal of Electron Microscopy **53** (2004), 451–458. https://doi.org/10.1093/jmicro/dfh080
28. T.L. Burnett, R. Kelley, B. Winiarski, L. Contreras, M. Daly, A. Gholinia, M.G. Burke, P.J. Withers, Large volume serial section tomography by Xe Plasma FIB dual beam microscopy, Ultramicroscopy **161** (2016), 119-129. https://doi.org/10.1016/j.ultramic.2015.11.001
29. T. Sato, K. Nakano, H. Matsumoto, S. Torikawa, I. Nakatani, M. Kiyohara and T. Isshiki, High quality lamella preparation of gallium nitride compound semiconductor using Triple Beam system, J. Phys.: Conf. Ser. **902** (2017), 012019. https://doi.org/10.1088/1742-6596/902/1/012019
30. J.F. Ziegler, The Stopping and Ranges of Ions in Matter, Pergamon (1977). https://doi.org/10.1016/C2013-0-00699-8
31. J.F. Ziegler, SRIM-2013. http://www.srim.org/ (accessed May 17, 2023)
32. P. J. Phillips, M. De Graef, L. Kovarik, A. Agrawal, W. Windl, and M. J. Mills, Ultramicroscopy **116**, 47–55 (2012). https://doi.org/10.1016/j.ultramic.2012.03.013
33. J. Uzuhashi, J. Chen, A. Kumar, W. Yi, T. Ohkubo, R. Tanaka, S. Takashima, M. Edo, K. Sierakowski, M. Bockowski, H. Sakurai, T. Kachi, T. Sekiguchi, and K. Hono, Atomic-scale investigation of implanted Mg in GaN through ultra-high-pressure annealing, J. Appl. Phys. 131, 185701 (2022). https://doi.org/10.1063/5.0087248

34. A. Lotnyk, D. Poppitz, U. Ross, J.W. Gerlach, F. Frost, S. Bernütz, E. Thelander, B. Rauschenbach, Focused high- and low-energy ion milling for TEM specimen preparation, Microelectronics Reliability **55**, 2119-2125 (2015). https://doi.org/10.1016/j.microrel.2015.07.005